Article

A novel DNA cascade reaction with high-efficiency target conversion for ultrasensitive electrochemiluminescence microRNA detection

Xinya Jiang, Huijun Wang, Ya-qin Chai, Hang Li, Wenbing Shi, and Ruo Yuan

Anal. Chem., **Just Accepted Manuscript** • DOI: 10.1021/acs.analchem.9b02404 • Publication Date (Web): 08 Jul 2019

A novel DNA cascade reaction with high-efficiency target conversion for ultrasensitive electrochemiluminescence microRNA detection

Xinya Jiang[a,b], Huijun Wang[a,b], Yaqin Chai[a], Hang Li[a], Wenbing Shi[b,*], Ruo Yuan[a,*]

[a] *Key Laboratory of Luminescent and Real-Time Analytical Chemistry (Southwest University), Ministry of Education, College of Chemistry and Chemical Engineering, Southwest University, Chongqing 400715, P. R. China*

[b] *Chongqing Key Laboratory of Inorganic Special Functional Materials, College of Chemistry and Chemical Engineering, Yangtze Normal University, Fuling, Chongqing 408100, P. R. China*

[*] Corresponding author. Tel.: +86-23-68252277; Fax: +86-23-68253172.

E-mail address: swb02182001@126.com (W.B. Shi); yuanruo@swu.edu.cn (R. Yuan),

Abstract

DNA amplification strategy has been a valuable tool for improving the sensitivity of biosensor. However, the freely diffusing reactants in most DNA amplification strategies limit the rate of DNA reaction, which further affect the amplification efficiency with unsatisfactory sensitivity. In present work, a novel localized DNA cascade reaction (LDCR) in a DNA nanomachine was designed for high-efficiency target conversion to construct electrochemiluminescence (ECL) biosensor for ultrasensitive microRNA-21 detection. The DNA nanomachine was constructed by using three footholds DNA scaffold to immobilize two metastable hairpins and reporter probe and confine them in a localized space. In the presence of microRNA-21, it initiated the LDCR and produced large amounts of mimic target (ferrocene labeled DNA, Fc-DNA) due to the locality effect. Thus, sensitive detection of microRNA-21 could be realized since Fc could effectively quench the ECL intensity of graphitic carbon nitride nanosheets (CNNS) due to the energy and electron transfer from excited-state of CNNS to oxidized species of Fc. Moreover, compared with other two developed DNA cascade reactions with freely diffusing reactants, the proposed LDCR benefits for shortening the reaction time and improving the amplification efficiency with enhanced sensitivity of the biosensor. Therefore, the proposed LDCR could be used as a highly efficient amplification strategy for ultrasensitive determination of biomarkers with low-abundance, which may promote the diagnostic efficiency of disease.

Introduction

Malignant tumors are one of the main reasons for increasing global mortality, which seriously threaten human health and social development[1,2]. MicroRNAs are a class of endogenous, non-coding small RNAs of approximately 20-24 nucleotides in length that regulate more than 60% of gene expression and participate in cell division, differentiation, apoptosis, and immune processes[3-5]. Recent studies have shown that the occurrence and development of many malignant tumors such as cancer, cardiovascular disease and neurological diseases are closely related to the abnormal expression of microRNAs[6-8]. However, some microRNAs with low-abundance in cells are difficult to be detected, so it is necessary to develop new and sensitive analytical method to meet the accurate detection of trace microRNAs in cells, which may has important significance for strengthening research and diagnosis of malignant tumors.

Until now, a great number of biosensors have been developed for the detection of biomarkers using electrochemiluminescence (ECL) technique due to its advantages of no additional light source, simple operation, sensitive detection, low background signal, etc[9-11]. In order to ameliorate the sensitivity of ECL biosensor, most amplification strategies, such as nanomaterial amplification[12,13], biological auxiliary amplification[14,15] and energy transfer amplification[16,17], are employed in the construction of biosensor. Among the biological auxiliary amplification strategies, DNA amplification strategy has attracted much attention in bioanalysis due to its exquisite specificity, predictability, and diversity[18-21]. Generally, the kinetics of DNA

hybridization so far depends almost on the diffusible DNA reactants that interact and collide randomly in a three-dimensional fluidic space[22,23]. Thus, the efficiency and rate of most DNA hybridization reactions are greatly retarded and prolonged as the DNA hybridization process needs seeking for next DNA hybridizing probe ceaselessly. Therefore, it is imperative to design new DNA hybridization reaction with accelerated reaction rate and efficiency for further bioanalysis application.

Recent several studies have begun to investigate the kinetics of DNA hybridization reaction *via* confining successive DNA reactants in a localized space, resulting in an increase in DNA reaction rate as well as improved reaction efficiency. For example, DNA origami scaffold with high precision has been utilized to localize DNA reactants for DNA strand displacement reaction (SDR)[24,25] and hydribization chain reaction (HCR)[26] with accelerated reaction rate. However, the application of DNA origami scaffold still remains challenging for its assembly requires precise positioning to achieve the efficient interaction between DNA reactants as a minor mismatch may halt the DNA reaction. Recently, Ren et al. employed DNA nanowire produced by rolling circle amplification to interval hybrid hairpin DNA probe pairs and thus realized the accelerated HCR for efficient fluorescence analysis[27]. Engelen et al employed DNA functionalized benzene-1,3,5- tricarboxamide polymers as scaffold to colocalize DNA reactants and achieved the acceleration of HCR, catalyzed hairpin assembly (CHA), and multiple input AND gates[28]. However, the participation of exotic enzyme and synthesis of DNA functionalized benzene-1,3,5-tricarboxamide polymers complicate the whole DNA reaction process. Inspired by this, we used a

simple self-assembly method to prepare a three footholds DNA scaffold for colocalizing DNA reactants to obtain localized DNA cascade reaction (LDCR) with accelerated reaction rate and high reaction efficiency for sensitive ECL biosensing.

MircoRNA-21 is demonstrated to be a potentially reliable biomarker due to its high expression in many tumors[29,30]. Therefore, quantification and identification is imperative for microRNA-21. In this study, an ultrasensitive ECL microRNA-21 biosensor was fabricated based on a novel LDCR amplification strategy that using three footholds DNA scaffold to immobilize two metastable hairpins and reporter probe and confine them in a localized space, which shortened the reaction time and improved the efficiency of target conversion. As illustrated in Scheme 1A, the three footholds DNA scaffold was generated by cross hydridization of three single-stranded DNA (L1, L2 and L3). Then, two metastable hairpins (HP1, HP2) and reporter probe (Rep, the hybridization product of single-stranded DNA (L4) and ferrocene labeled DNA (Fc-DNA)) respectively anchored at the corresponding footholds. In the presence of target microRNA-21, HP1 and HP2 were catalyzed to undergo a CHA reaction and a duplex structure was formed accompanied with the recycling of target microRNA-21. Immediately, DNA SDR occurred as the activated toehold d on HP2 allowed Rep to bind, resulting in the release of mimic target Fc-DNA. Due to the LDCR for high-efficiency target conversion, abundant mimic target Fc-DNA could be obtained, which further hybridized with capture probe and then quenched the ECL emission of graphitic carbon nitride nanosheets (CNNS), realizing sensitive detection of microRNA-21. The results indicated that the proposed ECL biosensor could

achieve sensitive detection of microRNA-21 with a low detection limit of 10.7 aM, suggesting that the proposed method created a novel promising detection platform for trace biomarker ultrasensitive detection.

Experimental Section

Assembly of three footholds DNA scaffold (TFDS) and DNA nanomachine

First, the TFDS was prepared by annealing three single-stranded DNA (L1, L2, and L3) in DNA hybridization buffer with the concentration of 5 μM at 95 ^{o}C for 5 min. Meanwhile, reporter probe (Rep) containing L4 and ferrocene modified L5 (Fc-DNA), HP1, and HP2 were also annealed for 5 min at 95 ^{o}C to form a double-stranded and hairpin structure, respectively. Then, the DNA nanomachine (TFDS-HP1-HP2-Rep) could be obtained by mixing TFDS (50 μL, 5 μM), HP1 (50 μL, 5 μM), HP2 (50 μL, 5 μM), and Rep (50 μL, 5 μM) solution and maintaining at 37 ^{o}C for 3 h. In addition, the comparative DNA nanomachine of TFDS-HP1 was prepared by mixing TFDS (50 μL, 5 μM), HP1 (50 μL, 5 μM) and 100 μL hybridization buffer and maintaining at 37 ^{o}C for 3 h. The another comparative DNA nanomachine of TFDS-HP1-HP2 was prepared by mixing TFDS (50 μL, 5 μM), HP1 (50 μL, 5 μM), HP2 (50 μL, 5 μM) and 50 μL hybridization buffer and maintaining at 37 ^{o}C for 3 h.

Preparation of mimic target Fc-DNA based on LDCR

The preparation of mimic target Fc-DNA was depicted in Scheme 1A. For easy separation of mimic target Fc-DNA, Au nanoparticles functionalized Fe_3O_4 magnetic

beads were synthesized ($Au@Fe_3O_4$, seen in the Supporting Information) as platform to load the as-prepared DNA nanomachine *via* Au-N bond. In the present of target microRNA-21, it bound to toehold a on HP1, resulting in the release of toeholds of b' and c' on HP1 *via* branch migration. Then, the activated toeholds of b' and c' on HP1 allowed the HP2 to bind. With the invasion of H2, an unstable ternary complex could be formed. Due to strand displacement principle, the unstable ternary complex finally reformed into steady state of HP1:HP2, resulting in the release of target microRNA-21 which could bind to a new HP1 and initiate another target cycle process. Meanwhile, the activated toehold of d on HP2 allowed the Rep to bind. Ultimately, with the invasion of Rep, the mimic target Fc-DNA could be released and obtained under magnetic separation. With the aid of LDCR for target cycle, large amounts of mimic target Fc-DNA would be obtained for further detection.

Synthesis of Pt modified graphitic carbon nitride nanosheets (CNNS-Pt)

First of all, the bulk graphitic carbon nitride (CN) was synthesized according to a previous method with some modification[31]. Concretely, the yellow bulk CN could be obtained by one-step thermal condensation of melamine at 520 ^oC for 4 h with a ramp time of 10 ^oC/min in a muffle furnace. For preparation of CNNS, 10 mg of bulk CN was first dispersed in 2 mL of ultrapure water. The obtained suspension was grinded mechanically by manual mortar-and-pestle for 2 h. After that, the resultant milky slurry was readily transferred to 8 mL of ultrapure water by manual shaking. Then, the formed suspension was centrifuged at 5000 rmp to remove large precipitates and thus CNNS was obtained. Then, 15 μL of H_2PtCl_6 (2%) was added into 2 mL of

CNNS solution, followed by continuously stirring for 6 h. Afterward, 50 μL of 10 mM sodium citrate solution was immediately added into above mixture. After stirring for 30 min, 200 μL of 10 mM newly prepared $NaBH_4$ solution was added into above mixture quickly. An additional of 30 min stirring was provided for complete reaction. Finally, the CNNS-Pt nanomaterial could be obtained by centrifugation and washing the above obtained mixture for three times with ultrapure water. The synthesized CNNS-Pt nanomaterial was redispersed in ultrapure water (1 mL) and stored at 4 °C. The synthetic process of CNNS-Pt nanomaterial was showed in Scheme 1C.

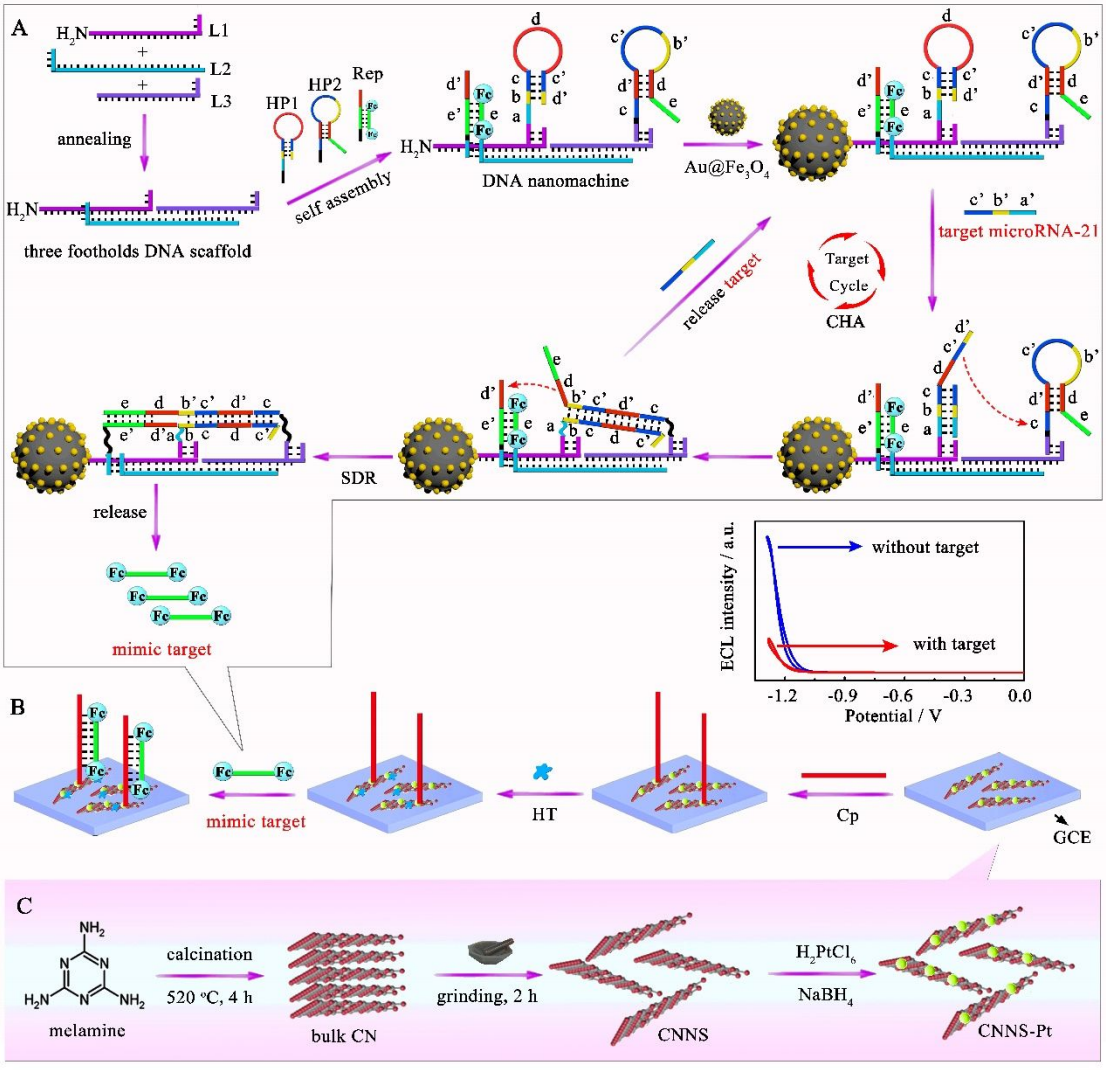

Scheme 1. Schematic illustration of the preparation of mimic target Fc-DNA based on

LDCR (A), the assembly process of the ECL biosensor (B), and the preparation of CNNS-Pt nanomaterial (C).

Construction of the ECL biosensor

The bare glassy carbon electrode (GCE, Φ = 4 mm) was burnished with 0.3, 0.05 μm alumina slurry, rinsed and sonicated with ethanol and ultrapure water. The GCE was then subjected to 5 μL of CNNS-Pt suspension and dried naturally to form a uniform film (CNNS-Pt/GCE). Followed that, 10 μL of 1.25 μM amino-terminated capture probe (Cp) was incubated on the CNNS-Pt/GCE for 12 h at 4 ^{o}C to obtain Cp modified GCE *via* Pt-N bond (Cp/CNNS-Pt/GCE). Then, 10 μL of 1.0 mM HT was incubated on the Cp/CNNS-Pt/GCE for 40 min to block the nonspecific adsorption sites (HT/Cp/CNNS-Pt/GCE). Finally, the as-prepared ECL biosensor was stored at 4 ^{o}C when not in use. The fabrication of the ECL biosensor was displayed in Scheme 1B.

ECL Detection procedure

For ECL detection of target microRNA-21, different concentrations of microRNA-21 were respectively added into the as-synthesized DNA nanomachine to obtain different concentrations of mimic target Fc-DNA after reaction for 80 min at 37 ^{o}C. The ECL signal of as-prepared biosensor was detected in an ECL detector cell containing 2 mL of supporting electrolyte under the potential scanning of -1.3 V to 0 V. With increasing concentration of microRNA-21, the amount of mimic target Fc-DNA increased, resulting in more Fc-DNA immobilized on electrode surface with

obvious decline of ECL signal. Therefore, sensitive detection of microRNA-21 could be achieved.

Gel electrophoresis analysis

The successful formation of DNA nanomachine and the DNA cascade reaction were verified by 16% polyacrylamide gel electrophoresis (PAGE) analysis. The loading sample containing 10 μL of DNA sample and 2 μL of loading buffer was injected into fresh polyacrylamide gel. Then, the obtained polyacrylamide gel ran in 1 × TBE buffer at constant current of 70 A for 2.5 h. After staining with gel-red for 15 min, Molecular Imager Gel Doc XR (BIO-RAD, U.S.A.) was utilized to scan the dyed polyacrylamide gel.

Results and Discussion

Characterization of CNNS and CNNS-Pt nanomaterials

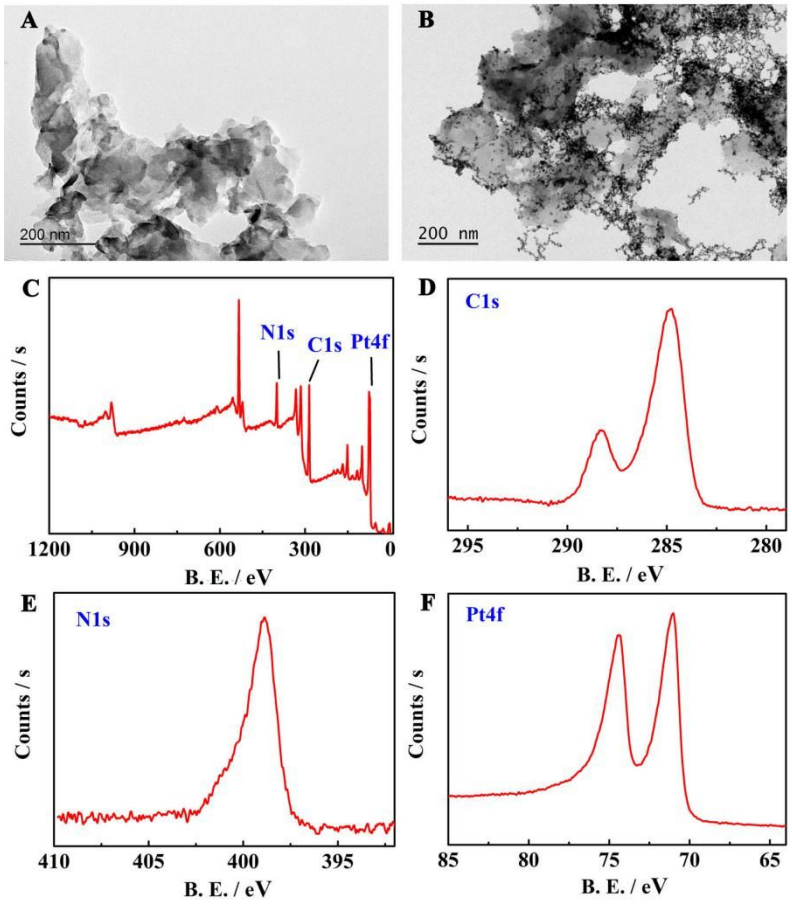

Figure 1. TEM images of CNNS (A) and CNNS-Pt (B). XPS analysis for (C) full region of CNNS-Pt, (D) C 1s region, (E) N 1s region, and (F) Pt 4f region.

The morphologies of CNNS and CNNS-Pt were characterized by TEM. The TEM image showed in Figure 1A indicated that CNNS was nanosheet-like structure, and the almost transparent characteristic of the nanosheet revealed its ultrathin thickness. The TEM image showed in Figure 1B depicted that a large number of black dots corresponding to Pt nanoparticles with average size of ca. 5 nm were anchored on CNNS surface. In addition, to further demonstrate the successful preparation of CNNS-Pt, elemental composition analysis was performed by a powerful XPS technique. The wide-scan survey spectrum of CNNS-Pt was presented in Figure 1C, in which the characteristic peaks of Pt 4f, N 1s, C 1s were clearly observed,

respectively. The Pt 4f located at 71.15 eV revealed that Pt nanoparticles were effectively attached on CNNS surface and atomic percentage of Pt in CNNS-Pt provided by XPS is 7.74%. Furthermore, Figure 1D, E, F were the amplified spectra of C 1s, N 1s, and Pt 4f, respectively.

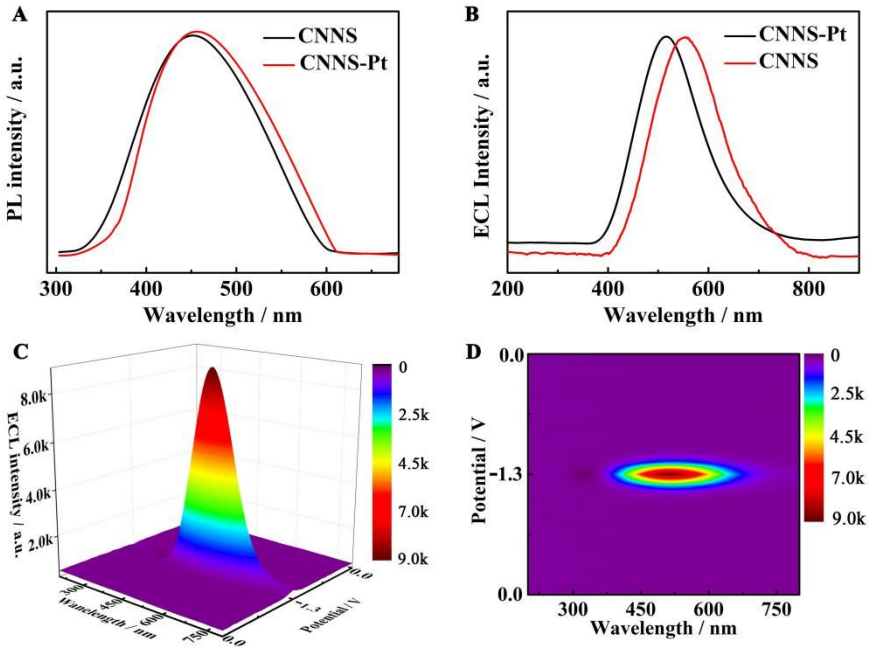

Figure 2. (A) Normalized FL spectra of CNNS and CNNS-Pt. (B) Normalized ECL spectra of CNNS and CNNS-Pt. (C) ECL 3D color map surface and (D) heat map image of CNNS-Pt in supporting electrolyte.

The optical properties of the prepared CNNS and CNNS-Pt nanomaterials were characterized by fluorescence (FL) and ECL techniques. Figure 2A showed the FL spectra of CNNS and CNNS-Pt. By comparing the FL spectra of CNNS (black line) with that of CNNS-Pt (red line), the loading of Pt nanoparticles on CNNS almost did not alter the original FL of CNNS. Figure 2B dispalyed the ECL spectra of CNNS and CNNS-Pt, revealing that the maximum ECL emission peak of CNNS-Pt (black line)

located at 515 nm which had a slight 38 nm blue-shift compared with the maximum ECL emission peak of CNNS (red line) owing to the quantum size effect[32]. Furthermore, Figure 2C was the ECL 3D color map surface of CNNS-Pt, which traced the ECL emission evolution process from 0 V to -1.3 V, then to 0 V. Figure 2D was its corresponding ECL heat map image of CNNS-Pt, from which we could intuitively observe that the maximum emission wavelength also located at 515 nm under the potential of -1.3 V.

PAGE characterization of DNA nanomachine and DNA cascade reaction

The designed DNA nanomachine and DNA cascade reaction were verified by gel electrophoresis, and the results were displayed in Figure 3. As depicted in Figure 3A, the bands in lanes a-c respectively corresponded to L1, L2, and L3, the bands in lanes e-g respectively corresponded to HP1, HP2, and Rep. The obvious new band with high molecular weight obtained in line d indicated that the TFDS could be formed by mixing L1, L2 and L3. Furthermore, a higher molecular weight band observed in line h suggested that HP1, HP2 and Rep immobilized on the TFDS. These results indicated that the designed DNA nanomachine could be synthesized successfully. In addition, the feasibility of DNA cascade reaction was displayed in Figure 3B, in which HP1, HP2 and Rep only had one band, respectively (lanes a-c). Compared with lane d, an obvious new band appeared in lane e after the addition of microRNA-21, indicating that DNA cascade reaction occurred and formed a new complex with high molecular weight.

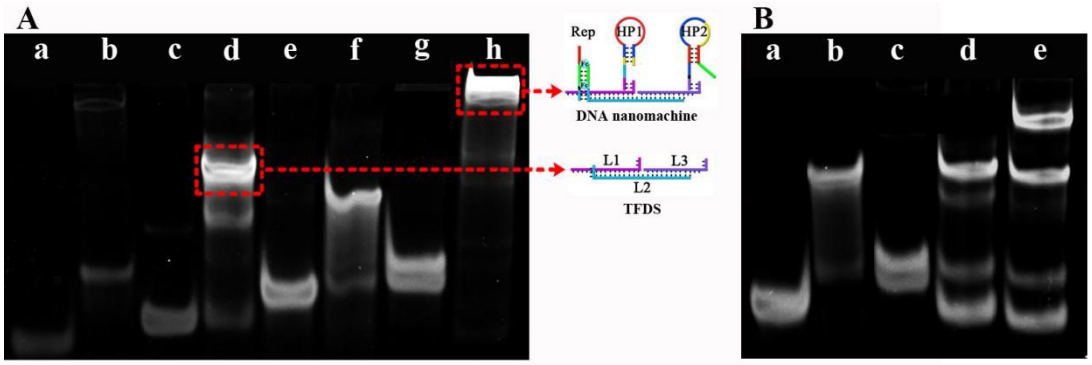

Figure 3. (A) PAGE analysis of DNA nanomachine preparation: lane a-h represent L1, L2, L3, TFDS, HP1, HP2, Rep, DNA nanomachine. (B) PAGE analysis of DNA cascade reaction: lane a-e represent HP1, HP2, Rep, HP1-HP2-Rep, HP1-HP2-Rep-micro RNA-21.

ECL behaviors of the enhancing and quenching process

To study the enhancing effect of Pt on ECL of CNNS, the signals of CNNS and CNNS-Pt were measured in PBS without and with 10 mM $S_2O_8^2$. As displayed in Figure 4A, the CNNS showed a weak ECL emission in PBS (curve a), while CNNS-Pt exhibited a higher ECL signal (curve b) due to the excellent conductivity of Pt. Moreover, an extremely strong ECL signal (ca. 17000 a.u.) was obtained from CNNS-Pt (curve d) in PBS containing 10 mM $S_2O_8^{2-}$ as coreactant when compared with CNNS (curve c, ca. 9000 a.u.). The reason could be ascribed to that Pt as co-reaction accelerator can expedite the electrocatalytic reduction of $S_2O_8^{2-}$ to produce more abundant $SO_4^{\bullet -}$ free radical for the ECL reaction of CNNS with obviously enhanced ECL signal. In addition, the quenching effect of Fc on CNNS-Pt was also investigated, as depicted in Figure 4B. The curve a in Figure 4B showed that CNNS-Pt had a strong ECL signal. However, the ECL intensity of CNNS-Pt reduced

largely in presence of 0.5 mg mL^{-1} Fc (curve b), and further reduced in presence of 1 mg mL^{-1} Fc(curve c). The results indicated that the ECL singal of CNNS-Pt could be effectively quenched by Fc due to the reason that the energy and electron transfer from excited-state of CNNS to Fc^{+} (oxidized species of Fc) restrain the radical reactions[33].

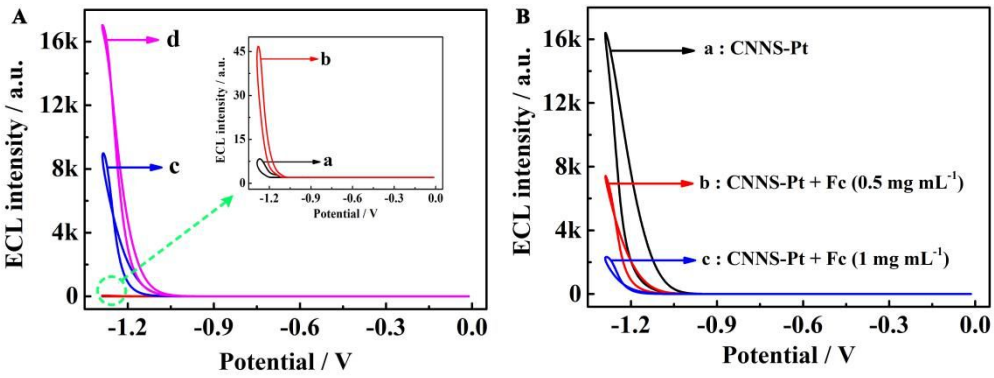

Figure 4. (A) ECL profiles of CNNS (a), CNNS-Pt (b) detected in PBS and ECL profiles of CNNS (c) and CNNS-Pt (d) detected in PBS containing 10 mM $S_2O_8^{2-}$. (B) ECL profiles of CNNS-Pt (a), CNNS-Pt with 0.5 mg mL^{-1} Fc (b), and CNNS-Pt with 1 mg mL^{-1} Fc (c) detected in PBS containing 10 mM $S_2O_8^{2-}$.

Optimization of the target microRNA-21 incubation time

In order to obtain the optimal analytical performance, we optimized the incubation time of target microRNA-21 before the ECL test. Figure 5A displayed the ECL intensity corresponding to various time periods with 1 pM microRNA-21. From the figure we can see that the ECL signal reduced gradually along with increasing microRNA-21 incubation time from 20 to 80 min. Then, the ECL intensity kept almost the same value in the range of 80-160 min. Therefore, the optimum incubation

time of target microRNA-21 was chosen to be 80 min for shortening the required time for target conversion.

Investigation the amplification and acceleration effect of the proposed LDCR

To study the amplification and acceleration efficiency of the proposed LDCR, three kinds of DNA nanomachines for target conversion were fabricated and used to carry out the time-dependent ECL analysis with 1 pM microRNA-21. The three kinds of DNA nanomachines were: (a) only HP1 was immobilized on TFDS (TFDS-HP1), (b) HP1 and HP2 were immobilized on TFDS (TFDS-HP1-HP2), and (c) HP1, HP2 and Rep were all immobilized on TFDS (TFDS-HP1-HP2-Rep, proposed DNA nanomachine). As depicted in Figure 5B, along with increasing incubation time of microRNA-21, the ECL intensities obtained from the three kinds of DNA nanomachines all reduced accordingly. However, compared with TFDS-HP1 and TFDS-HP1-HP2, TFDS-HP1-HP2-Rep resulted in the largest ECL decrease with same microRNA-21 concentration, indicating that the proposed LDCR exhibited a superior amplification effect. Furthermore, the completion time for TFDS-HP1-HP2-Rep was about 80 min, while 140 min and 100 min for TFDS-HP1 and TFDS-HP1-HP2, respectively, revealing that the proposed LDCR exhibited an excellent acceleration effect. In a word, the proposed LDCR amplification strategy could largely increase the detection sensitivity and greatly shorten the reaction time.

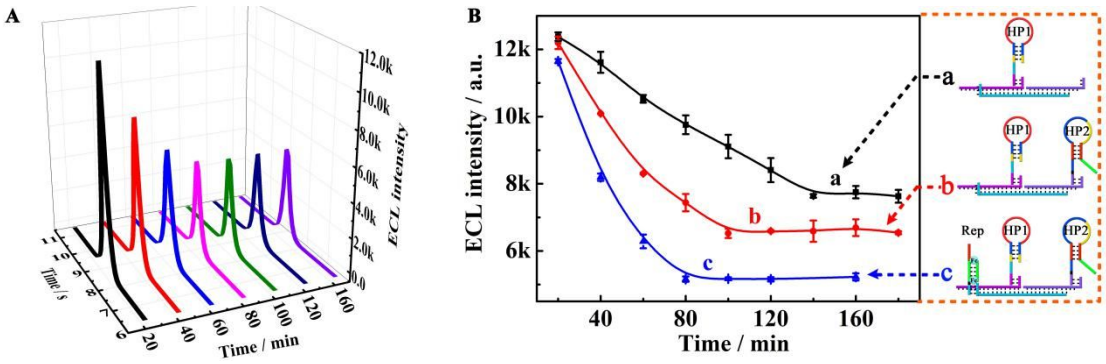

Figure 5. (A) Optimum reaction time for preparation mimic target Fc-DNA. (B) Investigation the amplification and acceleration effect of different DNA nanomachines: (a) TFDS-HP1, (b) TFDS-HP1-HP2, (c) TFDS-HP1-HP2-Rep (proposed DNA nanoprobe).

Calibration curve for miRNA-21 detection

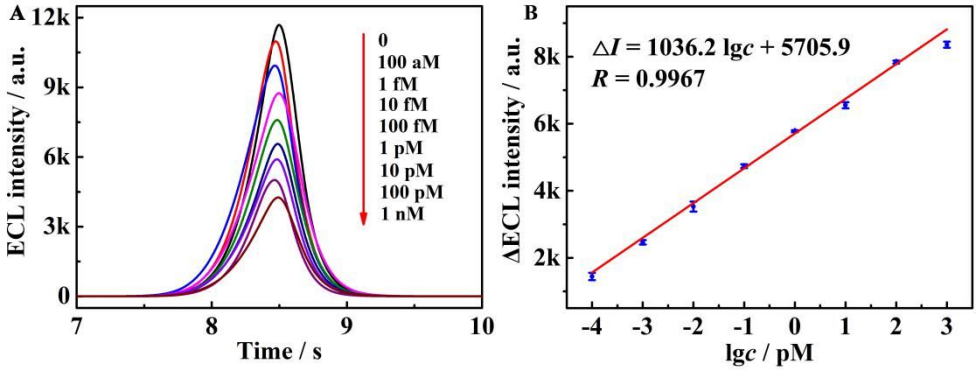

Figure 6. (A) ECL profiles of the LDCR amplification strategy based biosensor with various concentrations of microRNA-21. (B) Corresponding calibration curve of ΔI_{ECL} vs. lg$c$.

To investigate the analytical performance of the LDCR amplification strategy based ECL biosensor for microRNA-21, the ECL responses of the biosensor with various concentrations of microRNA-21 were recorded in the range of 100 aM to 1

nM. The results shown in Figure 6A suggested that the ECL signal decreased in turn as the concentration of microRNA-21 increased. The reason was ascribed to that large amounts of mimic target Fc-DNA could be obtained in the presence of high concentration of microRNA-21, resulting in obvious quenching effect on ECL of CNNS-Pt. Figure 6B was its corresponding calibration curve, in which the changes in ECL intensities (ΔI_{ECL}) acted as a function of the logarithm values of microRNA-21 concentration (lg$c$). As a result, the linear equation was ΔI_{ECL} = 1036.2 lg c + 5705.9, the regression coefficient (R) was 0.9967. In addition, the limit of detection was estimated to be 10.7 aM (S/N = 3). Compared with reported biosensor for microRNA-21 detection (see Table 1), the results manifested that the ECL biosensor based on the LDCR amplification strategy exhibited a more sensitive detection for microRNA-21.

Table 1. Reported detection methods for miRNA-21.

Method	Detection range	Detection limit	References
FL	10 fM - 500 fM	3 fM	34
DPV	5 fM - 5 pM	1.92 fM	35
PEC	0.25 fM - 0.25 nM	83 aM	36
SERS	10 fM - 10 nM	2.33 fM	37
ECL	10 fM - 0.1 nM	6.6 fM	38
ECL	1 fM - 1 nM	0.5 fM	39
ECL	100 aM - 1 nM	10.7 aM	This work

Other performance of the LDCR amplification strategy based ECL biosensor

Stability, reproducibility and selectivity are the three important parameters to evaluate a biosensor. In this study, the ECL emission of the proposed biosensor under continuous potential scanning for 15 cycles was recorded to investigate its stability. As displayed in Figure 7A, the proposed ECL biosensor possessed an outstanding stability which was presumably due to the stable luminescence performance of CNNS-Pt, and the relative standard deviation (RSD) was estimated to be 0.87%. For reproducibility investigation, six proposed ECL biosensor that fabricated in different batches received semblable ECL signal with a RSD less than 5%, implying acceptable reproducibility of the biosensor.

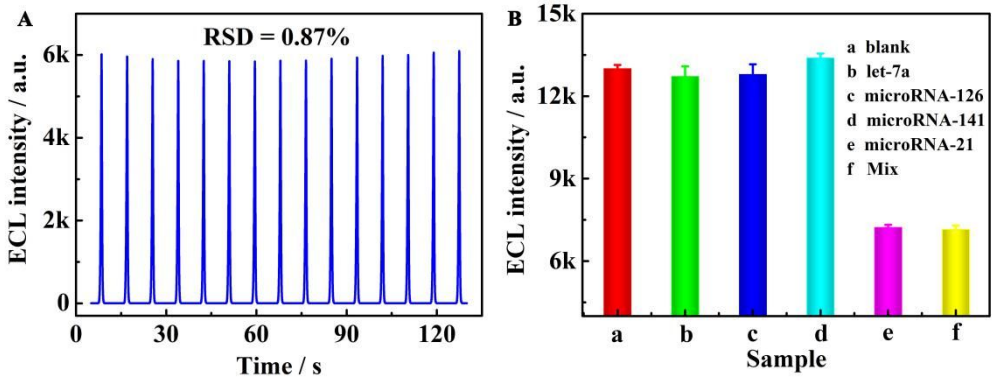

Figure. 7. ECL intensity of the proposed ECL biosensor under continuous potential scanning for 15 cycles (A) and with different interfering targets (B).

Additionally, let-7a, microRNA-126, and microRNA-142 were employed as interfering substances to evaluate the anti-interference ability of proposed ECL biosensor. As depicted in Figure 7B, compared with blank sample, 1 pM microRNA-21 would cause a significant decrease in ECL signal of the proposed

biosensor. However, let-7a, microRNA-126, and microRNA-142 with the concentration of 1 pM did not cause any noticeable ECL signal change. Identically, the mix sample containing 1 pM let-7a, microRNA-126, microRNA-142 and microRNA-21 also exhibited an obvious decrease in ECL intensity, and the obtained ECL intensity was similar with that obtained from pure microRNA-21 (1 pM). The results illustrated an excellent selectivity of the proposed ECL biosensor.

Preliminary analysis of the ECL biosensor in cancer cells

To study the application of the developed ECL biosensor based on LDCR amplification strategy, we applied it to detect microRNA-21 in cervical cancer cells (Hela) lysates with low expresion of microRNA-21 and human breast cancer cells (MCF-7) lysate with high expresion of microRNA-21. As shown in Figure 8, whether in Hela or MCF-7 lysate, the ECL signal gradually increased in turn as the number of cell increased. In Hela cell lysate, the ECL intensity tardily enhanced in the range of 10 to 10^6 cells, while the ECL intensity enhanced rapidly in the same number of MCF-7 cell lysate. This revealed that the proposed ECL biosensor could achieve the monitoring of microRNA expression in cancer cells.

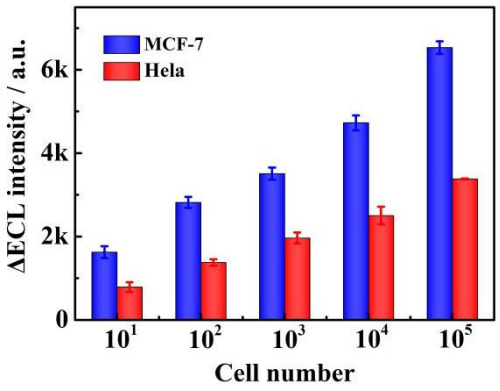

Figure 8. Application of the prepared ECL biosensor in Hela and MCF-7 lysates.

Conclusions

In conclusion, we designed a novel amplification strategy for construction of ultrasensitive ECL microRNA biosensor based on a LDCR in a DNA nanomachine which confined two metastable hairpins and reporter probe on TFDS. Compared with the conventional DNA cascade reactions with freely diffusing reactants, the proposed LDCR exhibited its own advantages. First, it could be expediently synthesized by a simple self-assembly method. Second, it greatly shortened the reaction time as the successive DNA reactants were confined in a localized space. Third, it improved the reaction efficiency with enhanced detection sensitivity down to 10.7 aM. With these advantages, the proposed amplification strategy could be utilized as a versatile and effective method for detection of biomarkers and disease prevention.

ASSOCIATED CONTENT

Supporting Information

The Supporting Information is available free of charge *via* the Internet at http://pubs.acs.org/.

Reagents and Apparatus, preparation of $Au@Fe_3O_4$, characterization of the ECL biosensor.

AUTHOR INFORMATION

Corresponding Authors

*Phone: +86-23-72793565. Fax: +86-23-72790008. E-mail: swb02182001@126.com

*Phone: +86-23-68252277. Fax: +86-23-68253172. E-mail: yuanruo@swu.edu.cn

ACKNOWLEDGEMENTS

This work was financially supported by the NNSF of China (21675129, 21775124, 21575116), the China Postdoctoral Science Foundation (2019M653817XB), and the Fundamental Research Funds for the Central Universities (XDJK2018AA003), China.

REFERENCES

(1) Bray, F.; Ferlay, J.; Soerjomataram, I.; Siegel, R. L.; Torre, L. A.; Jemal, A. *Ca-Cancer J. Clin.* **2018**, 68, 394-424.

(2) Ferlay, J.; Soerjomataram, I.; Dikshit, R.; Eser, S.; Mathers, C.; Rebelo, M.; Parkin, D. M.; Forman, D.; Bray, F. *Int. J. Cancer*, **2015**, 136, E359-E386.

(3) Calin, G. A.; Croce, C. M. *Nat. Rev. Cancer*, **2006**, 6, 857-866.

(4) Feinberg, M. W.; Moore, K. J. *Circ. Res.* **2016**, 118, 703-720.

(5) Wang, H.; Tang, H. R.; Yang, C.; Li, Y. X. *Anal. Chem.* **2019**, DOI: 10.1021/acs.analchem.9b02025.

(6) Lin, S. B.; Gregory, R. I. *Nat. Rev. Cancer*, **2015**, 15, 321-333.

(7) Barwari, T.; Joshi, A.; Mayr, M. *J. Am. Coll. Cardiol.* **2016**, 68, 2577-2584.

(8) Miao, X. M.; Cheng, Z. Y.;, Ma, H. Y.; Li, Z. B.; Xue, N.; Wang, P. *Anal. Chem.* **2018**, 90, 1098-1103.

(9) Ye, J.; Zhu, L. P.; Yan, M. X.; Zhu, Q. J.; Lu, Q. Q.; Huang, J. S.; Cui, H.; Yang,

X. R. *Anal. Chem.* **2018**, *91*, 1524-1531.

(10) Feng, Y. Q.; Sun, F.; Wang, N. N.; Lei, J. P.; Ju, H. X. *Anal. Chem.* **2017**, 89, 7659-7666.

(11) Zhao, G. h.; Wang, Y. G.; Li, X. J.; Yue, Q.; Dong, X.; Du, B.; Cao, W.; Wei, Q. *Anal. Chem*. **2019**, 91, 1989-1996.

(12) Wang, S. S.; Zhao, Y. Y.; Wang, M. M.; Li, H. J.; Saqib, M.; Ge, C. H.; Zhang, X. D.; Jin, Y. D. *Anal. Chem*. **2019**, 91, 3048-3054.

(13) Zhang, R.; Zhong, X.; Chen, A. Y.; Liu, J. L.; Li, S. K.; Chai, Y.; Zhuo, Y.; Yuan, R. *Anal. Chem*. **2019**, 91, 3681-3686.

(14) Lu, L. P.; Wang, J. X.; Miao, W. J.; Wang, X. Y.; Guo, G. S. *Anal. Chem.* **2019**, 91, 1452-1459.

(15) Ge, J. J.; Zhao, Y.; Li, C. L.; Jie, G. F. *Anal. Chem*. **2019**, 91, 3546-3554.

(16) Chen, M. M.; Wang, Y.; Cheng, S. B.; Wen, W.; Zhang, X. H.; Wang, S. F.; Huang, W. H. *Anal. Chem.* **2018**, 90, 5075-5081.

(17) Cao, J. T.; Liu, F. R.; Fu, X. L.; Ma, J. X.; Ren, S. W.; Liu, Y. M. *Chem. Commun*. **2019**, 55, 2829-2832.

(18) Liu, W.; Chen, A. Y.; Li, S. K.; Peng, K. F.; Chai, Y. Q.; Yuan, R. *Anal. Chem.* **2019**, 91, 1516-1523.

(19) Zhang, N.; Shi, X. M.; Guo, H. Q.; Zhao, X. Z.; Zhao, W. W.; Xu, J. J.; Chen, H. Y. *Anal. Chem.* **2018**, 90, 11892-11898.

(20) Xu, Z. Q.; Chang, Y. Y.; Chai, Y. Q.; Wang, H. J.; Yuan, R. *Anal. Chem.* **2019**, 91, 4883-4888.

(21) Feng, Q.; Wang, M. Y.; Zhao, X. L.; Wang, P. *Langmuir*, **2018**, 34, 10153-10162.

(22) Li, L.; Feng, J.; Liu, H. Y.; Li, Q. L.; Tong, L. L.; Tang, B. *Chem. Sci.* **2016**, 7, 1940-1945.

(23) Jiang, Y.; Li, B. L.; Milligan, J. N.; Bhadra, S.; Ellington, A. D. *J. Am. Chem. Soc.* **2013**, 135, 7430-7433.

(24) Bui, H.; Shah, S.; Mokhtar, R.; Song, T. Q.; Garg, S.; Reif, J. *ACS Nano*, **2018**, 12, 1146-1155.

(25) Teichmann, M.; Kopperger, E.; Simmel, F. C. *ACS Nano*, **2014**, 8, 8487-8496.

(26) Chatterjee, G.; Dalchau, N.; Muscat, R. A.; Phillips, A.; Seelig, G. *Nat. Nanotech.* **2017**, 12, 920.

(27) Ren, K.; Xu, Y. F.; Liu, Y.; Yang, M.; Ju, H. X. *ACS Nano*, **2017**, 12, 263-271.

(28) Engelen, W.; Wijnands, S. P.; Merkx, M. *J. Am. Chem. Soc.* **2018**, 140, 9758-9767.

(29) Ramanujam, D. P.; Hinkel, R.; Kazcmarek, V.; Howe, A.; Klett, K.; Dueck, A.; Thum, T.; Laugwitz, K. L.; Kupatt, C.; Engelhardt, S. *Circ. Res.* **2018**, 123, A553-A553.

(30) Shi, C. Z.; Yang, Y. Z.; Xia, Y.; Okugawa, Y.; Yang, J.; Liang, Y.; Chen, H. Q.; Zhang, P.; Wang, F.; Han, H. Z.; Wu, W.; Gao, R. Y,; Gasche, C.; Qin, H. L.; Ma, Y. L.; Goel, A. *Gut*, **2016**, 65, 1470-1481.

(31) Ji, J. J.; Wen, J.; Shen, Y. F.; Lv, Y. Q.; Chen, Y. L.; Liu, S. Q.; Ma, H. B.; Zhang, Y. J. *J. Am. Chem. Soc.* **2017**, 139, 11698-11701.

(32) Zhang, J. S.; Chen, Y.; Wang, X. C. *Energy Environ. Sci.* **2015**, 8, 3092-3108.

(33) Deng, S. Y.; Lei, J. P.; Liu, Y.; Huang, Y.; Ju, H. X. *Chem. Commun.* **2013**, 49, 2106-2108.

(34) Xia, Y. K.; Wang, L. L.; Li, J.; Chen, X. Q.; Lan, J. M.; Yan, A.; Lei, Y.; Yang,

S.; Yang, H. H.; Chen, J. H. *Anal. Chem.* **2018**, 90, 8969-8976.

(35) Zhang, K.; Dong, H. F.; Dai, W. H.; Meng, X. D.; Lu, H. T.; Wu, T. T.; Zhang, X. J. *Anal. Chem.* **2017**, 89, 648-655.

(36) Zheng, Y. N.; Liang, W. B.; Xiong, C. Y.; Yuan, Y. L.; Chai, Y. Q.; Yuan, R. *Anal. Chem.* **2016**, 88, 8698-8705.

(37) Wang, Z. X.; Ye, S. J.; Zhang, N.; Liu, X.; Wang, M. L. *Anal. Chem.* **2019**, 91, 5043-5050.

(38) Zhang, P.; Jiang, J.; Yuan, R.; Zhuo, Y.; Chai, Y. Q. *J. Am. Chem. Soc.* **2018**, 140, 9361-9364.

(39) Feng, Q. M.; Shen, Y. Z.; Li, M. X.; Zhang, Z. L.; Zhao, W.; Xu, J. J.; Chen, H. Y. *Anal Chem*. **2016**, 88, 937-944.

For TOC Only

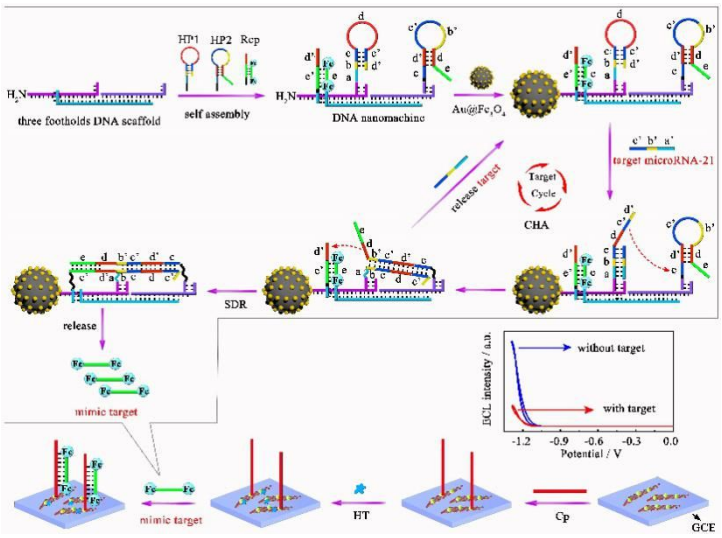
HP1
HP2
Rep
three footholds DNA scaffold
self assembly
DNA nanomachine
Au@Fe3O4
target microRNA-21
release target
Target Cycle
CHA
SDR
release
mimic target
without target
with target
ECL intensity / a.u.
Potential / V
HT
Cp
GCE